Synthesis and characterization of nano-zinc oxide fiber: adsorption of acid blue 92 dye, isotherms, thermodynamics and kinetics

Deepro Sanjid Qais
Dhaka University
Md Nazrul Islam
Dhaka University
Mohd. Hafiz Dzarfan Othman
Universiti Teknologi Malaysia
H.N.M. Ekramul Mahmud
Universiti Malaya
Md. Emran Quayum
Dhaka University
Md Anwarul Islam
Dhaka University
Iqbal Mohammad Ibrahim Ismail
King Abdulaziz University Faculty of Sciences
Ahsan Habib (habibchem@du.ac.bd)
Dhaka University

Research Article

Keywords: Nano-ZnO fiber, Polyethylene glycol (PEG), Azo dye, Adsorption isotherms and kinetics, Chemisorption, Water treatment

Posted Date: April 7th, 2022

DOI: https://doi.org/10.21203/rs.3.rs-1530081/v1

Synthesis and characterization of nano-zinc oxide fiber: adsorption of acid blue 92 dye, isotherms, thermodynamics and kinetics

Abstract

Rapid industrialization, particularly textile/dyeing, causes substantial surface water contamination by various dyes and pigments globally. Bangladesh's export-oriented textile industry has grown dramatically in recent decades, causing significant pollution of nearby water bodies. In this work, nano-zinc oxide was synthesized by a precipitation method with PEG 400 and characterized using SEM, XRD and FTIR techniques and found to be fiber-like, perfectly wurtzite and pure. The nano-ZnO was applied to remove acid blue 92, an ionic dye, from aqueous solution to investigate it as an adsorbent. The effects of pH, adsorbent dosage, AB92 concentration and contact time on adsorption process were investigated for optimization. According to the correlation coefficients (R^2) and the fitting of Redlich-Peterson model, the adsorption process followed Langmuir isotherm at lower temperature and Freundlich isotherm at higher temperature with Temkin model. The adsorption process was found to be endothermic and spontaneous. For adsorption thermodynamics, ΔH was found to be +20.32 $kJmol^{-1}$, and ΔG was varied from -1.86 to -3.84 $kJmol^{-1}$ as the temperature increased from 291 to 317 K. The adsorption kinetics exhibited pseudo second order. The Temkin isotherm and Elovich kinetic model suggested that the process to be chemisorption. The nano-ZnO showed tremendous re-usability as an adsorbent for the removal of AB92. The results are suggesting for designing nano-ZnO-based methods to remove organic pollutants efficiently from industrial effluents for ecological and sustainable development. The mechanisms of nano-ZnO fiber formation and anionic dye adsorption on nano-ZnO are also discussed.

Keywords: Nano-ZnO fiber; Polyethylene glycol (PEG); Azo dye; Adsorption isotherms and kinetics; Chemisorption; Water treatment.

1. Introduction

Bangladesh's economy is mainly based on textile industries that export. Export-oriented textile industries contributed 17.9% of gross domestic product (GDP) in 2010, and this figure is expected to rise to 25% by 2023. Textile industries, on the other hand, require large amounts of water as well as various chemicals in their processes, so they discharge huge amounts of effluents containing various contaminants, particularly synthetic dyes, into nearby water bodies (Habib et al., 2012a; Habib et al., 2012b; Muslim et al., 2012; Muslim et al., 2013; Hossain et al., 2016; Ertugay and Acar, 2017; Ahmadi et al., 2020). Despite the fact that Bangladesh's Department of Environment (DoE) has made it mandatory for each textile unit to have an effluent treatment plant (ETP), the ETP plants have not been functioning properly (Department of Environment, 2008).As a result, water bodies near the textile and dyeing industries are severely contaminated (Habib et al., 2012a; Habib et al., 2012b; Muslim et al., 2012; Muslim et al., 2013; Hossain et al., 2016).

Among the applications of chemicals in industrial processes, synthetic dyes have been widely used in various industries, including textile and dyeing (Doulati et al., 2008), leather, printing, paper, plastics, cosmetics, pharmaceuticals, petrochemicals, and so on (Benkhaya and El Harfi, 2017; Benkhaya et al., 2020). Synthetic dyes are manufactured and used in various industrial units at a rate of roughly 700,000 metric tons per year around the world (Hoda et al. 2006; Moussavi and Mahmoudi 2009; Balarak et al., 2021). About 60-70% of these synthetic dyes are used in textile industry (Lacasse and Baumann, 2004; Rawat et al., 2016; Brüschweilerand Merlot, 2017). It is worth mentioning that azo dyes are made up of aromatic amines (AAs), which are released through bacterial biotransformation when they come into dermal contact (Platzek et al., 1999;Freeman, 2013; Akhtar et al., 2016;Brüschweilerand Merlot, 2017; Amin et al., 2020). These AAs may have mutagenic and/or carcinogenic effects on humans (Platzek, 2010). As a result, several azo dyes which release the toxic AAs have been banned from textiles in the European Union (Annex XVII of the REACH regulation; No, 1907/2006) (EC, 2009) and in North America (Mo, 2020).

Only a small portion of the dyes are used for staining during the dyeing process, so a large amount is discharged into nearby water bodies as industrial effluents. To protect human health and the environment, it is therefore necessary to develop an efficient and cost-effective method for removing unstained azo dyes from industrial effluents. There have already been several methods developed for removing and/or mineralizing organic contaminants from industrial effluents. Among them, adsorption (Habib et al., 2006; Han et al., 2008; Ortega et al., 2017;

Ahmadi and Igwegbe 2020; Igwegbe et al. 2020), oxidation (Habib et al., 2012b; Muslim et al., 2013; Hossain et al., 2016; Ertugay and Acar, 2017; Ahmadi et al., 2018), photocatalytic degradation (Habib et al., 2012a; Muslim et al., 2012; Saravanan et al., 2013; Saravanan et al., 2014), coagulation-flocculation (Obiora-Okafo and Onukwuli, 2018; Somasundaran and Runkana, 2005) and microbial-based process (Tan et al., 2013; Agrawal et al., 2014, Govindwar et al., 2014; Tan et al., 2016) have proven to be the most effective methods. The adsorption method has been widely used to remove pollutants, particularly organic dyes, from aqueous solution because of its numerous advantages, including cost effectiveness, significant removal efficiency, and the absence of secondary pollution (Habib et al., 2006; Han et al., 2008; Moussavi and Mahmoudi, 2009; Gao et al. 2013; Ortega et al., 2017; Ahmadi and Igwegbe 2020; Igwegbe et al. 2020).

Metal oxides and metal nanoparticles, such as MgO, Fe_3O_4/MgO nanoparticles, nano-ZnO, Mn-nanoparticles, Ni/Fe and Mg/Fe layered double hydroxides, and modified-SiO_2 nanoparticles, have been utilized as adsorbents to remove dyes from aqueous solutions. Metal oxides and metal nanoparticles, such as MgO (Moussavi and Mahmoudi, 2009), Fe_3O_4/MgO nanoparticles (Salem et al., 2016), nano-ZnO (Lei et al., 2017; Zafar et al., 2019), Mn-nanoparticles (Arshadi et al., 2014), Ni/Fe and Mg/Fe layered double hydroxides (Elmoubarki et al., 2017), nanofibrous metal-organic membranes (Efome et al., 2018a; Efome et al., 2018b) and modified-SiO_2 nanoparticles (Patra et al., 2016) have been utilized as adsorbents to remove pollutants including dyes and metal ions from aqueous solutions. It is noted that nano-rod ZnO exhibited better adsorption efficiency compared to spherical ZnO for removal of the organic dyes (da Silva et al., 2021). Hence, attempts have been made to produce fiber-like nano-ZnO with a higher adsorption efficiency than rod-like and/or spherical nano-ZnO.

In this study, nano-ZnO fibers were synthesized using a precipitation method, and then characterized using scanning electron microscopy (SEM), X-ray diffraction (XRD), and Fourier transform-infrared spectroscopy (FT-IR) techniques. Under dark conditions, the as-prepared nano-ZnO was used to remove acid blue 92 (AB92) (Scheme 1), an anionic dye, from aqueous solution by varying dye concentration, adsorbent dosage, solution pH, and temperature. Cationic dyes such as methylene blue (MB) and rhodamine B (RB) were also used to compare the adsorption efficiencies of the nano-ZnO fibers for the anionic and cationic dyes under dark conditions.

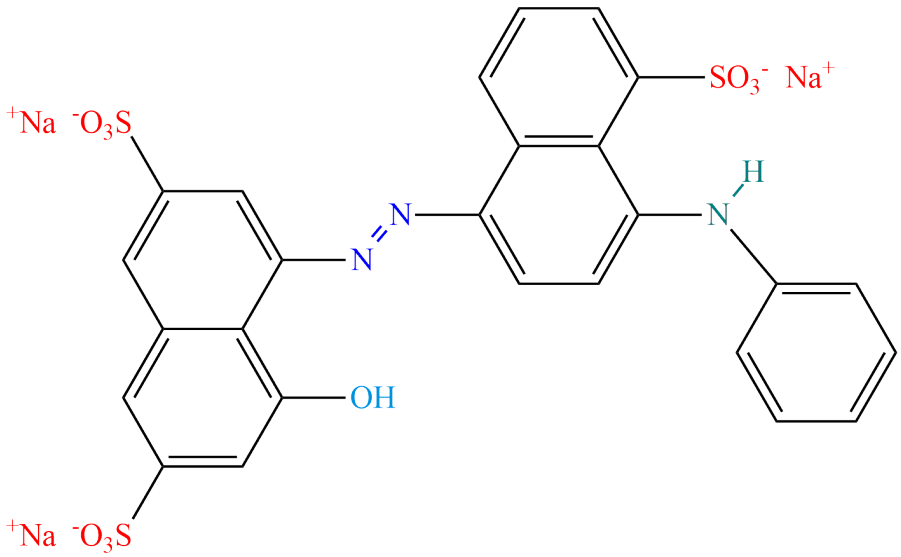

Scheme 1. Structure of acid blue 92 (AB92), trisodium 4-[(4-anilino-5-sulfonaphthalen-1-yl)diazinyl]-5-hydroxynaphthalene-2,7-disulfonate ($C_{26}H_{16}N_3O_{10}S_3Na_3$; M. Mass: 695.58).

2. Experimental

2.1 *Materials*

Acid blue 92 (AB92) dye (Scheme 1) was collected from the local dye suppliers. The adsorption maximum, λ_{max}, of AB92 is 570 nm. Hydrochloric acid, sodium chloride, ammonia and polyethylene glycol 400 (PEG 400) solution were purchased from Merck, Darmstadt, Germany. All the chemicals were used without further purification. Distilled water was used all over the experiments.

2.2*Synthesis and characterization of nano-ZnO*

Fiber-like nano-zinc oxide was precipitated from zinc nitrate solution by adding ammonia solution in the presence of 1% PEG 400. The precipitate ZnO was washed with distilled water at least three times and air dried. The air dried ZnO precipitate was placed in a desiccator filled with silica gel to remove water completely. The obtained zinc oxide was characterized using scanning electron microscope (SEM: model S-3400N, Hitachi, Tokyo, Japan), X-ray diffraction (XRD: Bruker DB-Advance X-ray diffractometer, Germany) and Fourier Transform infrared (FTIR: IR-Prestige 21 Shimadzu, Japan) techniques.

2.3*Synthesis of dye solution*

Some amount of AB92 dye was taken in a 50 mL volumetric flask in order to make a concentrated dye solution. A small volume of the stock solution was pipetted out and poured in a 100 mL volumetric flask and filled up to the mark with distilled water. Concentration of AB92 dye solution was calculated through recording the absorbance at λ_{max} = 570 nm,

absorption maxima of AB92, using a UV-Vis spectrophotometer (UV-160A, Shimadzu Corporation, Kyoto, Japan). The final dye concentration was obtained from the absorbance using the molar absorptivity determined from the Beer-Lambert's equation:

$$A = \varepsilon cl \quad (1)$$

where, A is absorbance, ε is molar absorptivity of AB92 (ε = 17,500 $Lmol^{-1}cm^{-1}$), l is the cell constant (1 cm) and c is the concentration of AB92.

2.4 Adsorption procedure

The dye concentration, adsorbent dosage, pH, and temperature were all varied in a series of experiments where just one parameter was changed while the others remained constant. The dye concentration and adsorbent dosage were varied within a range from 25.43 to 67.34 mgL^{-1} at 1.00 gL^{-1} of nano-ZnO and 0.40 to 3.00 gL^{-1} at 45.32 mgL^{-1} of AB92, respectively where solution pH 7.0 at 298 K. Solution pH and temperature were also varied ranging from 5.0 to 9.0 at 298 K and 291 to 317 K at pH 7.0, respectively with dye concentration of 45.32 mgL^{-1} and adsorbent dosage of 1.00 gL^{-1}. This is because ZnO dissolves at low solution pH, for example ≤ 4.5. All the experiments were carried out under dark conditions.

2.5 Adsorption efficiency and equilibrium adsorption quantity

Adsorption efficiency in percent removal (%) was calculated using equation (2) while equation (3) was used to calculate the equilibrium adsorption quantity (q_e).

$$Removal\ (\%) = \frac{c_0 - c_t}{c_0} \times 100 \quad (2)$$

$$Adsorption\ quantity\ (q_e) = \frac{c_0 - c_t}{W} \times V \quad (3)$$

where c_0 and c_t are initial and at time t dye concentration, respectively where q_e is the equilibrium adsorption quantity, V is volume of the experimental solution (100 mL) and W is the amount of ZnO.

2.6 *Adsorption isotherms*

The experimental data were fitted into Langmuir, Freundlich, Redlich-Peterson, and Temkin's adsorption isotherm models in order to optimize the adsorption process using equations (4), (5), (6), and (7) respectively (Zhang et al., 2020; Belhachemi et al., 2011; Nethaji et al. 2013; Ngakou et al., 2019).

$$q_e = \frac{q_m K_L c_e}{1 + K_L c_e} \quad (4)$$

$$q_e = K_F c_e^{\frac{1}{n}} \quad (5)$$

$$q_e = \frac{A\, c_e}{1 + B\, {c_e}^g} \quad (6)$$

$$q_e = \frac{RT}{b_T}\, ln(A_T c_e) \quad (7)$$

where c_e is the equilibrium concentration of AB92, q_m (mgg^{-1}) is the maximum adsorption capacity of nano-ZnO fiber corresponding to monolayer formation where 'K_L' is a coefficient related to the energy of adsorption in the Langmuir isotherm. The K_F and n are the constants in Freundlich isotherm. K_F is the capacity of nano-ZnO for multilayer adsorption of AB92 and n is intensity of adsorption. Parameters A, B and g are the Redlich-Peterson isotherm constants used to determine whether the adsorption process follows the Langmuir or Freundlich isotherm. A_T (Lmg^{-1}) and b_T ($Jmol^{-1}$) are the Temkin constants. The terms 'b_T' is related to heat of adsorption and 'A_T' is the equilibrium binding constant corresponding to the maximum binding energy. R (8.314 J/molK) is the universal gas constant and T (K) is the absolute temperature (298 K). The values of the adsorption model parameters were calculated from the non-linear regression plot of q_e vs c_e.

2.7 Adsorption thermodynamics

The adsorption of AB92 onto the nano-ZnO fiber was studied at different temperatures in order to explore the effects of temperature on the adsorption process. The thermodynamic parameters such as enthalpy (ΔH), entropy (ΔS) and Gibb's free energy (ΔG) for the adsorption of AB92 onto the nano-ZnO fiber were calculated using the following equations 8-10 (Wu et al., 2019).

$$K_d = \frac{q_e}{c_e} \quad (8)$$

$$lnK_d = -\frac{\Delta H}{RT} + \frac{\Delta S}{R} \quad (9)$$

where K_d stands for thermodynamic equilibrium constant.

$$\Delta G = \Delta H - T\Delta S \quad (10)$$

2.8 Adsorption kinetics

To explore the adsorption mechanism of AB92 dye onto the fiber-like nano-ZnO, pseudo-first order and pseudo-second order kinetic models were used. The experimental data was fitted into the Lagergren,Ho-Mckay kinetic models to evaluate whether the adsorption kinetics were pseudo first order (equ. 11) or pseudo second order (equ. 12). The Elovich model was implemented to study the rate of chemisorption (equ. 13). The rate equations can be written as follows (Zhang et al., 2020; López-Luna et al., 2019; Ngakou et al., 2019):

$$q_t = q_e(1 - e^{-k_1 t}) \quad (11)$$

$$q_t = \frac{k_2 {q_e}^2 t}{1 + k_2 q_e t} \quad (12)$$

$$q_t = \frac{1}{B} ln\,(1 + ABt) \quad (13)$$

where k_1 (min^{-1}) and k_2 ($gmg^{-1}min^{-1}$) are the adsorption rate constants of pseudo-first and pseudo-second order kinetic models, respectively, A and B are the initial rate of chemisorption and desorption for the Elovich kinetic model respectively, and q_t and q_e (both in mgg^{-1}) are the equilibrium adsorption uptake at time = t and t = ∞, respectively.

3. Results and discussion

3.1. *Characterization of nano-ZnO*

The SEM image, XRD pattern, and FTIR spectrum of the as-prepared nano-ZnO are shown in Figures 1(a), (b), and (c), respectively. As seen from Fig. 1, most of the prepared nano-ZnO is fiber-like and aggregated to some extent. Figure 1(b) depicts the XRD pattern of the as-prepared ZnO. The XRD pattern shows the characteristic peaks (100), (002), (101), (102), (110), (103), (112), (201) and (202) of pure ZnO. As shown in inset in Figure 1(b), the XRD results are in good agreement with the standard values of the wurtzite structure of ZnO (JCPDS: 36-1451) (Elmorsi et al., 2017). Therefore, it is concluded that the precipitation method with 1% PEG 400 aided the formation of fiber-like nano-ZnO with perfectly wurtzite structure.

In a previous study, we attempted to fabricate rod-like nano-ZnO in the presence of surfactants such as sodium dodecyl sulfate (SDS), cetyl trimethyl ammonium bromide (CTAB), and triton X-100, and observed that SDS could control rod-like nano-ZnO formation (unpublished, Leila et al. 2018). During nucleation, anionic SDS molecules are thought to adsorb on the seed ZnO. The bulky group of the SDS molecules prevents further anionic SDS species from adsorbing from other sides, but it may allow the formation of unidirectional rod-like nano-ZnO. Because PEG and SDS are structurally distinct, their functions will differ.

In this study, PEG 400 was used to control the formation of various nanostructured ZnOs. PEG molecules in the precipitation method cause fiber-like nano-ZnO to form. Despite the fact that the exact mechanism of PEG-assisted nano-ZnO fiber formation is unknown, an arbitrary explanation based on literature and current findings is provided below (Parra et al., 2015; Pavani et al., 2015; Tshabalala et al., 2012; Dobryszycki et al., 2001; Li et al., 2003; Habib et al., 2020; Nargis et al., 2021; Wikipedia).

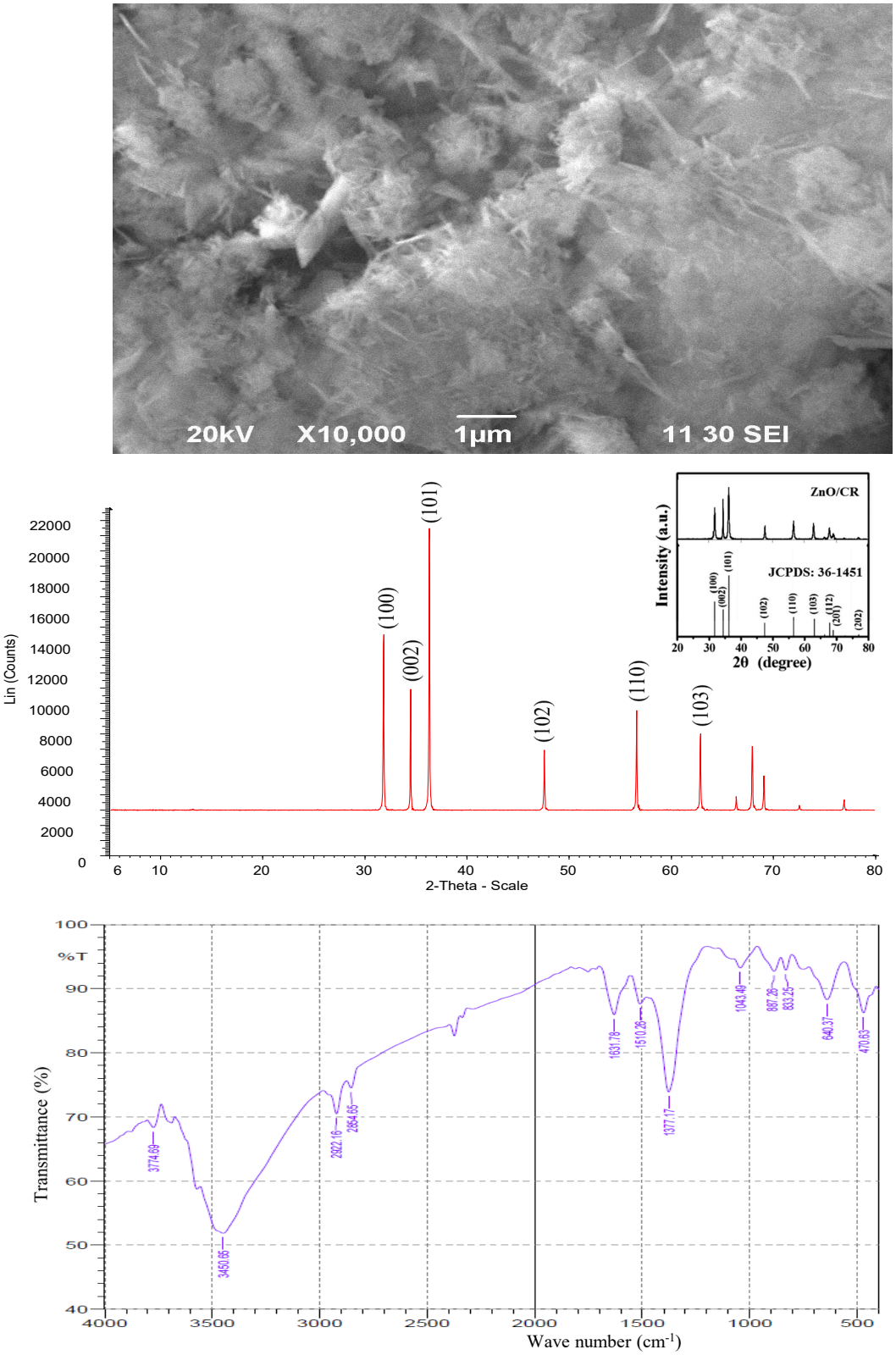

234

235 Figure 1. Characterization of the prepared nano-ZnO (a) SEM image, (b) XRD pattern and (c)

236 FTIR spectrum. Inset is for JCPDS:36-1451 of ZnO (Elmorsi et al., 2017).

237

In the wet chemical method, the PEG molecules are crucial for changing the nanostructures of ZnO particles from spherical to wire/rod-like (Parra et al., 2015; Pavani et al., 2015). PEG molecules with the formula [$H(OCH_2CH_2)_nOH$] are nonionic surfactants with a hydrophilic nonionic ether group (-O-) and a hydrophobic ethylene unit (-CH_2-CH_2-).Water molecules are associated with the nonionic ether group, -O-, due to a strong repelling tendency between water molecules and the hydrophobic ethylene, -CH_2-CH_2-,unit (Parra et al., 2015; Tshabalala et al., 2012). As a result, the PEG molecules self-assembled on the surface, with the hydrophilic end pointing toward the water molecule and the hydrophobic end pointing away from it.

Prior to discussing the mechanism of nano-ZnO fiber formation, it is necessary to consider the speciation of Zn(II) in the aqueous system. According to a speciation diagram, Zn(II) predominantly present (~90%) in aqueous solutionas$Zn(II)_{aq}$ ($[Zn(II)(H_2O)_6]^{2+}$) species at pH 6.9 and speciation data reveal the stepwise formation of $[Zn(H_2O)_{6-n}(OH)_n]^{2-n}$ species (*i.e.*,$Zn(OH)^{+}_{aq}$, $Zn(OH)_2{}^{0}_{aq}$, $Zn(OH)_3{}^{-}_{aq}$, $Zn(OH)_4{}^{2-}_{aq}$) with solution pH (Habib et al., 2020; Nargis et al., 2021). The cationic $Zn(II)_{aq}$ ion in acidic solution coordinated with the oxygen atom of the ether group due to electrostatic forces of attraction between the cationic $Zn(II)_{aq}$ ion and the lone pairs of electrons of the oxygen atom, remains Zn-O as a template unit for the crystal growth. Because the ether oxygen atom is more basic than the oxygen atom in water molecules, the Zn(II)aq ion prefers to coordinate with it. This can be explained by the fact that ether oxygen has a higher proton affinity (PA: 828.4 $kJmol^{-1}$) than water (PA: 703 $kJmol^{-1}$) (Wikipedia). With rising solution pH, stepwise deprotonation of the coordinated water molecules with the Zn(II) ion of the Zn-O template occurs. As a result, the template Zn(II) ion must have a hydroxyl group attached to it.

As previously stated, solution pH causes the formation of various hydroxozinc(II) species, which can exist as either soluble (aqua) or insoluble (colloids) forms depending on their solubility products. Both the soluble (aqua) and insoluble (colloids) forms of Zn(II) ion must carry hydroxyl groups and approach the Zn-O template due to hydrogen bonding between hydroxyl groups of incoming hydroxozinc(II) species and Zn-O template (Habib et al., 2020). With increasing solution pH, more colloidal ZnO(H) particles form and deposit on the Zn-O template. One-dimensional (1D) nano-ZnO crystal formation is enhanced by hydrophobic cone type ethylene units. Scheme 2 depicts a suggested mechanism for the formation of 1D crystal growth of nano-ZnO fiber. The length of the fiber-like ZnO depends on the degree of adsorption of the colloidal ZnO(H) particles on the Zn-O template (Parra et al., 2015; Pavani et al., 2015; Tshabalala et al., 2012). The amount of PEG and the length of its chain may cause structural deformation, resulting in fiber-like nano-ZnO. Since ZnO exhibits polar crystal growth along

[0 0 0 1] direction, rod-like and/or fiber-like nanostructures of ZnO are possible, as shown in Figure 1(a) (Parra et al., 2015; Pavani et al., 2015; Tshabalala et al., 2012).

Figure 1(c) shows the FT-IR spectrum of the as-prepared ZnO measured in the range of 4000-400 cm^{-1}. As shown in Figure 1(c), the prepared ZnO showed the vibrational peaks at 470, 640, 737, 833, 887, 1043, 1377, 1510, 1631, 2854, 2922 and 3450 cm^{-1}. The peak appearing at 470 cm^{-1} was attributed to the Zn-O stretching band while the vibrational peaks appeared within a range from 1700 to 600 cm^{-1} corresponding to C=O, C-O and C-H vibrations (Xiong et al., 2009). The peaks appeared within 2854- 3450 cm^{-1} were attributed to the O-H stretching vibrations and bending modes of adsorbed water molecules, respectively (Xiong et al., 2009). In the precipitation method, PEG was used as a capping agent in order to fabricate nano-ZnO fiber. The appearance of the C=O, C-O and C-H vibration bands in the IR spectrum was due to the presence of PEG.

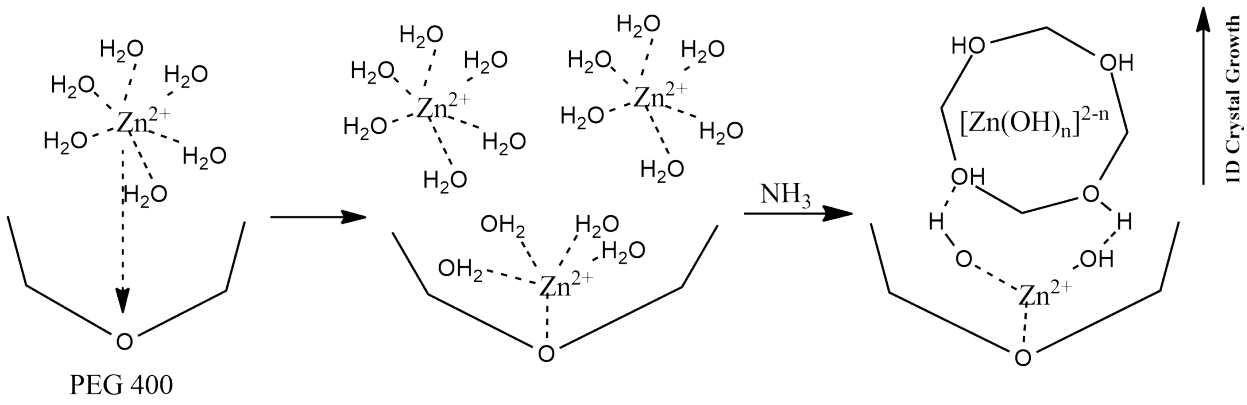

Scheme 2. A proposed mechanism of formation of nano-ZnO fiber by precipitation method in presence of PEG 400.

3.2. *Effect of initial dye concentrations*

The effect of initial dye concentrations on the adsorption of AB92 onto the nano-ZnO fiber was carried out to optimize the adsorbent dose and equilibrium time. Reasonably, the availability of surface area for adsorption will be maximum at the initial stage, particularly within the first 5 min, which results in significant adsorption efficiency. The extent of adsorption decreases with contact time as the adsorption process continues. The amount of adsorbent is being limited with time because adsorbate molecules occupy most of the active sites at the initial stage of the adsorption process. At a fixed amount of the adsorbent, the initial adsorbate concentration leads to different concentrations of adsorbate molecules on the active sites of adsorbents (Jethave et. al. 2018; Tang et. al. 2014).

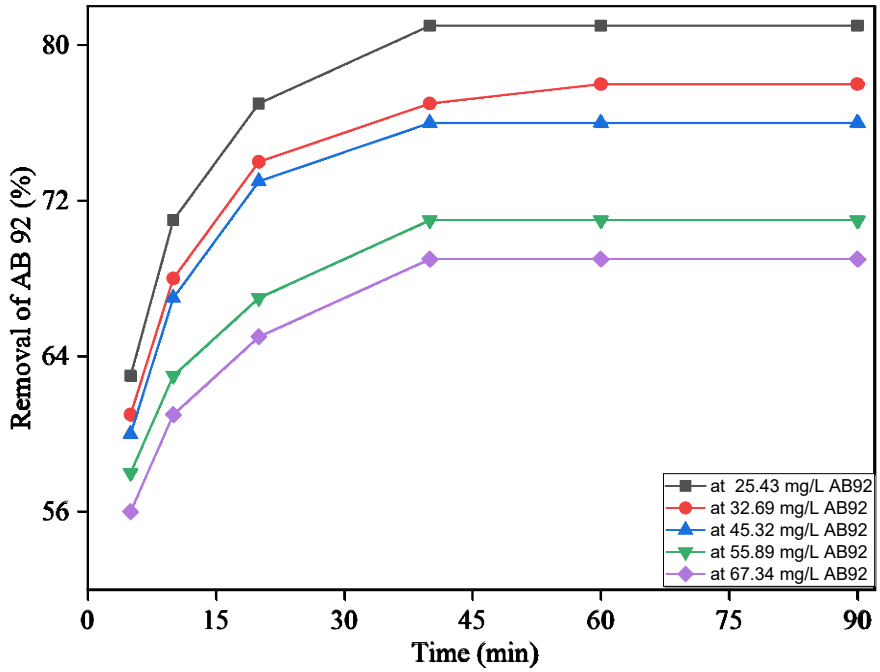

Figure 2. Effect of initial dye concentration on the removal of AB92 in the presence of 1 gL^{-1} of nano-ZnO fiber. Solution pH: 7.0; Temperature: 298 K.

Figure 2 shows the effect of initial concentrations of the AB92 dye in the presence of 1.00 gL^{-1} of nano-ZnO at solution pH 7.0 at 298 K. As shown in Figure 2, all the dye concentrations exhibited a sharp rise in adsorption, and the equilibrium conditions were attained at 40 min. After 40 min, no significant adsorption was observed. The low concentration of AB92 dye (25.43 mgL^{-1}) showed the maximum removal (81%) from aqueous solution while minimum removal (69%) was observed for the highest concentration (67.34 mgL^{-1}) of the AB92. It is reasonable to find the maximum removal of AB 92 for the lowest concentration (25.34 mgL^{-1}) of the dye in the presence of a fixed amount of the nano-ZnO.

3.2. *Effect of adsorbent dose*

Figure 3 depicts the effect of dose on the adsorption efficiency of AB 92. As seen from Figure 3, the removal efficiency of the AB 92 dyes increases with increase nano-ZnO. It is reasonable that the number of active sites for will be maximum at the higher amount of the adsorbent.

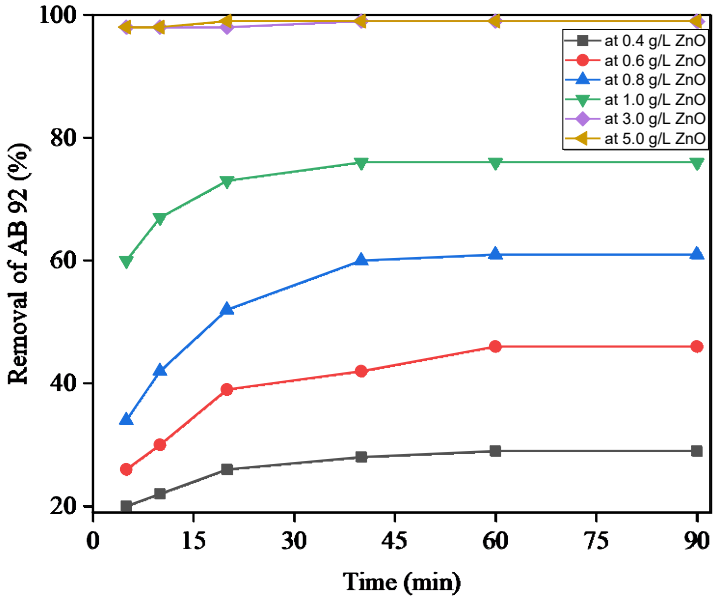

Figure 3. Effect of adsorbent dose on the removal of AB 92. [AB 92]: 45.32 mgL^{-1}; Solution pH: 7.0; Temperature: 298 K.

For 1.00 gL-1 of nano-ZnO fiber, the maximum removal of AB 92 was 78%, while for 0.40 gL-1 of nano-ZnO fiber, the maximum removal was only 29%. With higher adsorbent dosages, such as 3.00 gL-1, about 98% of AB 92 was removed in only 5 min. In the continued adsorption process, no further removal was observed. This is because a certain number of AB 92 dye molecules were completely adsorbed into comparable active sites on nano-ZnO surfaces, leaving an excess of active sites unoccupied (Habib et al., 2006; Hoda et al., 2006).

3.3. *Effect of pH*

Figure 4 shows the effect of solution pH on the removal of the AB 92 dye in the presence of the nano-ZnO fiber in aqueous solution at 298 K. As shown in Figure 4, the maximum removal (77%) was observed for the solution pH 8.0 followed by 76% for pH 7.0 at the equilibrium time (40 min), however that decreased either the solution pH increased or decreased.

The zero-point charge of nano-ZnO is 8.9, thus, the surface of the nano-ZnO remains positive, $Zn(OH)^{+}$, up to the solution pH ≤ 8.9 and then becomes negatively charged (ZnO^{-}) as the solution pH exceeds 8.9 (Degen and Kosec, 2000; Habib et al., 2012a). The pK_a value of the AB 92 dye is 11.22, so the dye molecules are supposed to exist as electrically neutral species in aqueous medium within the experimental pH range, 5.0 - 9.0. However, the sodiated AB 92 dye molecules are reasonably present as partially ionized form, $[AB\ 92]^{-}$ in the aqueous solution, where Na^{+} acts as a counter ion below the pK_a value, 11.22. The percentage of ionized

AB 92 dye molecules will be higher in the pH range from neutral to alkaline than in acidic pH. It is expected that the AB 92 dye molecules become positively charged through gaining proton (H^+) as the solution pH decreases from neutral to acidic. This is due to the presence of the azo group (-N=N-) in the AB 92 dye molecules. It is highly desirable that for the adsorption of the cationic dyes such as methylene blue (MB) and rhodamine B (RB) onto the nano-ZnO (1.00 gL^{-1}) should be minimum (~5%) at solution pH 7.0 at 298 K as shown in Figure 5. These results suggested that the surface charge of the prepared nano-ZnO was obviously positive at pH < 8.9 (*zpc* of nano-ZnO) and the adsorption of the cationic dyes, such as MB and RB, onto the nano-ZnO became negligible (~5%). In fact, the electrostatic force of repulsion between the two positively charged species is mainly responsible for the minimal adsorption of the cation dye molecules onto the positively charged surface of nano-ZnO at pH < 8.9.

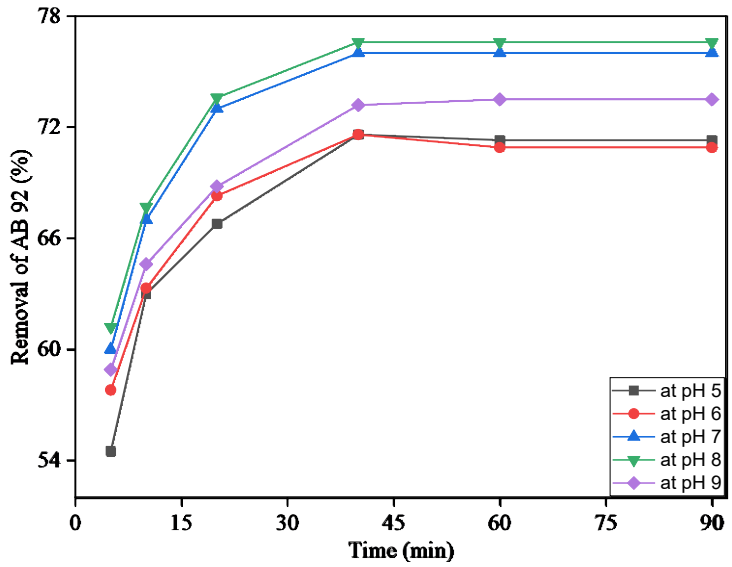

Figure 4. Effect of pH on the removal of AB 92 in the presence of nano-ZnO fiber (1.00 gL^{-1}). [AB 92]: 45.32 mgL^{-1}; Temperature: 298 K.

At low solution pH (5.0-6.0), a considerable fraction of the AB 92 dye molecules become positively charged, thus resulting in lower adsorption efficiency (removal, ~71%) of the cationic dye molecules onto the positively charged surface of the nano-ZnO at the equilibrium time, 40 min (Figure 4). At solution pH 9.0, the adsorption efficiency of the AB 92 dye onto the nano-ZnO was a little bit higher (removal, ~73%) compared to that for pH 5-6 at the equilibrium time. The *zpc* of the nano-ZnO is 8.9, reasonably most of the surface-active sites of the nano-ZnO will remain positively charged at the solution pH 9.0. The AB 92 dye molecules are mainly anionic at the solution pH 9.0 that may elevate the adsorption efficiency

slightly. Because of the dissolution of ZnO at low solution pH, the experiment was not carried out at lower pHs such as 4.0 or 3.0.

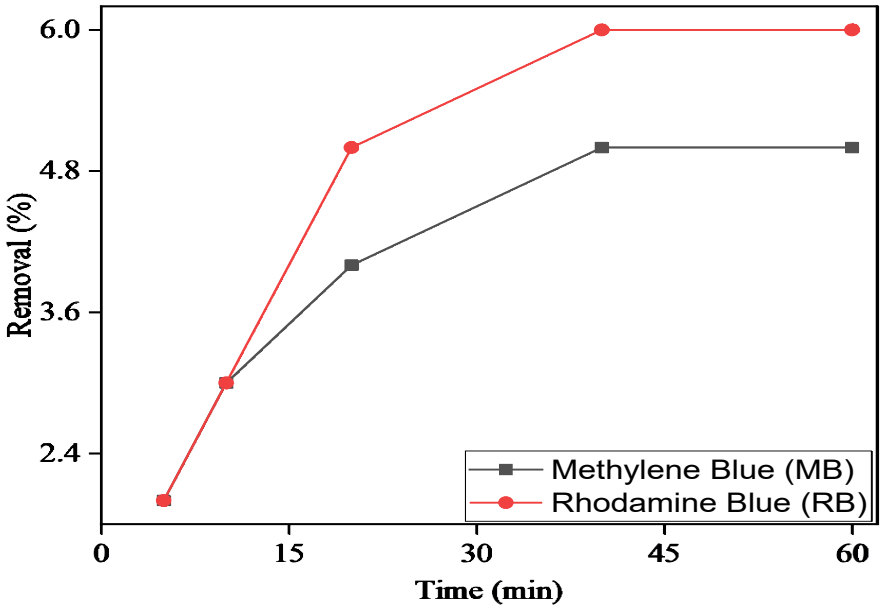

Figure 5. Removal of methylene blue (MB) and rhodamine B (RB) in the presence of nano-ZnO fiber (1.00 gL^{-1}), [Cationic dye]: 45.55 mgL^{-1}; Temperature: 298 K.

3.4. *Adsorption isotherms*

Adsorption isotherms are mathematical models that have been generated with the means of the experimental data. The isotherms describe the distribution of the adsorbate molecules onto the adsorbent surfaces through either physisorption and/or chemisorption. In this paper, The equilibrium data for AB 92 onto the nano-ZnO fiber was analyzed using the most generally used isotherms, such as the Langmuir, Freundlich, and Temkin models, in order to find a model that could be used for adsorption process design and optimization. The Langmuir isotherm stands for monolayer homogeneous adsorption (Langmuir, 1918) and the Freundlich isotherm is for heterogeneous multilayer (Freundlich, 1906) while the Redlich-Peterson isotherm combines both the Langmuir and Freundlich isotherms (Redlich and Peterson, 1959)and the Temkin isotherm is for chemisorption (Temkin and Pyzhev, 1940). The Langmuir, Freundlich, Redlich-Peterson and Temkin equations can be expressed using equations (4), (5), (6), and (7), respectively.

Figures 6(a), (b), (c) and (d) show the Langmuir, Freundlich, Redlich-Peterson and Temkin models, respectively. The isotherms parameters are tabulated in Table 1. According to these figures, Langmuir, Freundlich, Redlich-Peterson, and Temkin isotherms fitted the adsorption

data almost perfectly as the correlation coefficients (R^2) for all of the isotherms are quite close to unity at room temperature, 291K.However, when the temperature is raised, the adsorption data began to deviate from the Langmuir model, with R^2<0.95 at 311K. With increasing temperature, Langmuir's maximum adsorption quantity, q_m, decreases significantly.

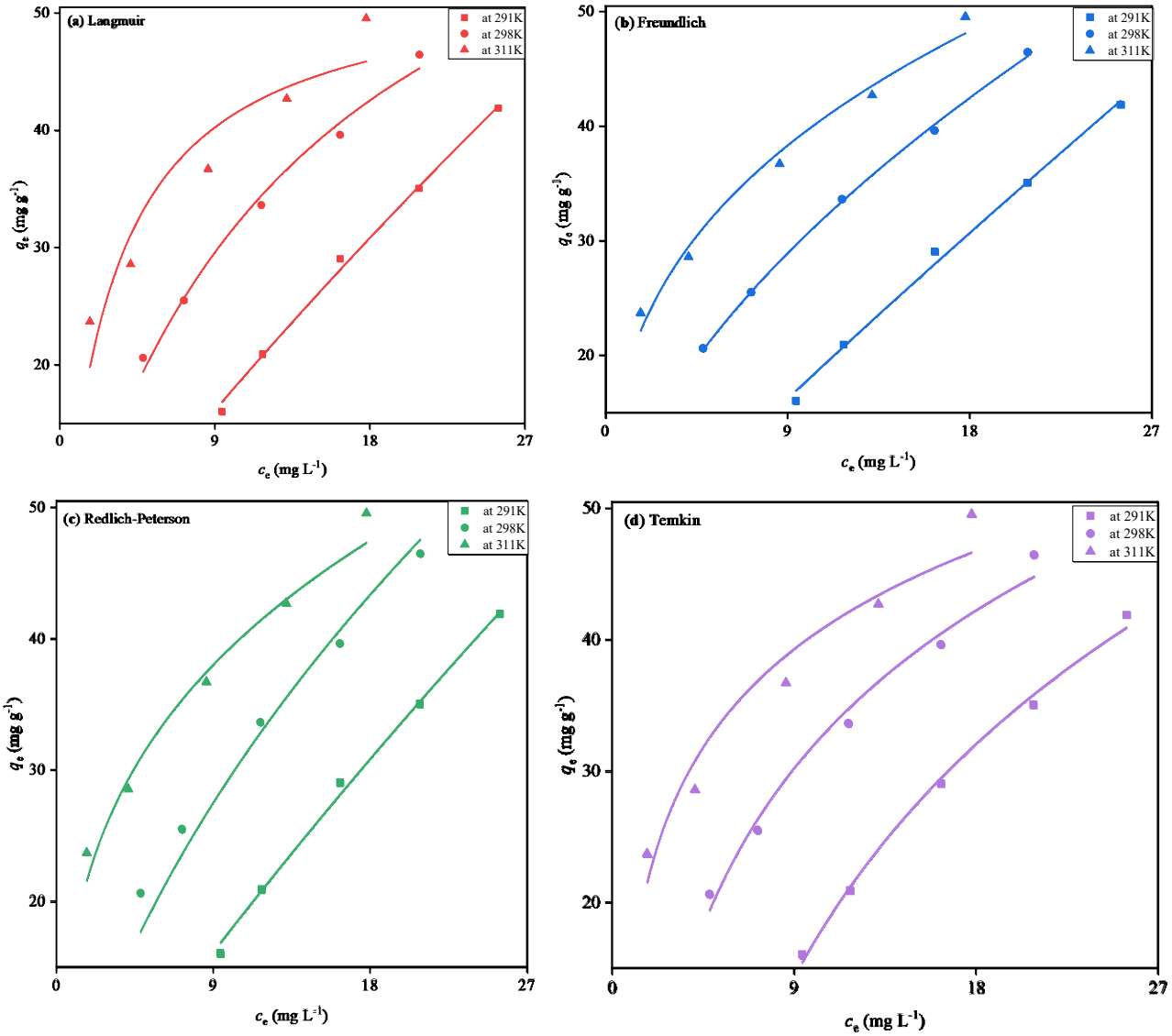

Figure 6. Adsorption isotherm plots of (a) Langmuir, (b) Freundlich, (c) Redlich-Peterson and (d) Temkin models at different temperatures. Nano-ZnO fiber: 1.00gL^{-1}; Solution pH: 7.0.

Table 1. Isotherm parameters of adsorption of AB 92 onto nano-ZnO fiber at different temperatures. Nano-ZnO: 1.00 g L^{-1}; Solution pH: 7.0.

Temp. (K)	Langmuir			Freundlich			Redlich-Peterson				Temkin		
	q_m (mgg^{-1})	K_L (Lg^{-1})	R^2	K_F ($mgg^{-1}((Lmg^{-1})^{1/n})^{-1}$)	1/n	R^2	A (Lg^{-1})	B (Lmg^{-1})	g	R^2	A_T (Lg-1)	b_T ($Jmol^{-1}$)	R^2
291	343.12	0.005	0.9964	2.15	0.92	0.9953	1.88	0.005	1.00	0.9963	0.19	94.46	0.9952
298	75.72	0.071	0.9894	8.54	0.56	0.9989	6.65	0.326	0.58	0.9652	0.63	142.67	0.9842
311	53.51	0.338	0.8953	18.41	0.33	0.9837	122.05	6.006	0.59	0.9754	4.21	239.25	0.9672

At lower temperatures, the adsorption process follows the Langmuir isotherm (Abdelkader et. al. 2015; Ahmadi et al., 2020; Belhachemi et al., 2011), but at higher temperatures, it follows the Freundlich isotherm (Malakootian et al., 2015; Salaimi et al., 2017a; Zafar et al., 2019; Sun et al., 2020; Yakar et al., 2020). In the Freundlich model, 1/n = 0 signifies irreversible, 1/n less than 1 indicates favorable, and 1/n greater than 1 indicates unfavorable (Zafar et al., 2019; Yakar et al., 2020). The 1/n decreased as the temperature increased, showing that the heterogeneous multilayer system became more favorable.

If the constant g in the Redlich-Peterson isotherm is unity or near to unity, the model will follow the Langmuir model; however, if the value moves away from unity and Bc_e^g is more than unity, the model will follow the Freundlich model (Wang et al., 2013; Belhachemi et al., 2011; Zhang et al., 2020). In Figure 6(c), g changed from 1 to 0.59 as the temperature increased from 291K to 311K. According to B in Table 1, Bc_e^g is greater than unity as well. This confirms that the adsorption process followed Langmuir model at lower temperatures but the process tends to follow Freundlich model more than Langmuir with increasing temperature. This indicates that the AB 92 dye molecules form homogenous monolayers at low temperatures and heterogeneous multilayers at higher temperatures onto the nano-ZnO fiber.

As demonstrated in Table 1, A_T and b_T increased with temperature, resulting in a greater chemical interaction between AB 92 molecules and nano-ZnO fiber surfaces, as predicted by the Temkin model. The adsorption process is caused by electrostatic force of attraction since AB 92 is an anionic dye and the surface charge of nano-ZnO is positive at pH 7.0 (Zhang et al., 2020; Belhachemi et al., 2011; Ngakou et al., 2019). Due to the positive surface charge, the maximum adsorption quantity of anionic dye AB 92 is quite high compared to that of cationic dye MB, which only exhibits around 10.70 mgg^{-1} (Zhang et. al., 2013). Based on the isotherm

data at various temperatures, it can be concluded that the adsorption of AB 92 onto the nano-ZnO fiber strongly follows Langmuir at lower temperatures, and that as the temperature rises, the inclination to follow Freundlich and Temkin increases and Langmuir diminishes.

3.5. *Adsorption thermodynamics*

Figure 7 showed that the adsorption efficiency of the AB92 dye on the nano-ZnO increases with increasing the solution temperature. As shown in Figure 7, thermal heating substantially enhanced the adsorption efficiency of the AB92 dye on the nano-ZnO compared to room temperature (Yakar et. al., 2020), but little enhancement was observed at the higher temperatures. It is noted that equilibrium was attained at 40 min, whereas desorption occurred at the highest temperature, 317 K. It is reasonable to observe a minor desorption of the adsorbed AB92 dye molecules at the elevated temperature, 317 K. This is because the nano-ZnO molecules may also absorb the thermal energy at the elevated temperature, 317 K, thus a slight desorption occurred.

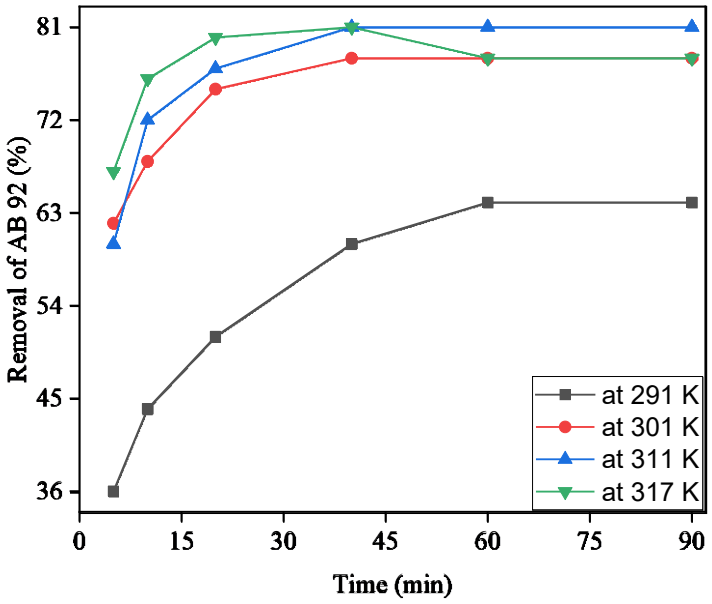

Figure 7. The effect of temperature on the adsorption efficiency of AB92 dye onto the nano-ZnO fiber surface. [AB92]: 45.32 mgL^{-1}; Nano-ZnO fiber: 1.00 gL^{-1}; Solution pH: 7.0.

The values of ΔH and ΔS were calculated from the slope and intercept of the plot of $\ln K_d$ versus T^{-1} as shown in Figure 8 and ΔG was obtained from equation 9, respectively. These thermodynamic parameters are tabulated in Table 2. The results showed that the values of ΔH and ΔS were found to be +20.32 $kJmol^{-1}$ and +76.21 $Jmol^{-1}K^{-1}$, respectively. These results revealed that the adsorption was endothermic in nature and dominated by chemisorption

(Duran et al., 2011; Li et al., 2014; Zafar et al., 2019). It is reasonable to realize that the AB 92 dye molecules were deposited onto the nano-ZnO fiber surface through chemisorption. Because the surface charge of nano-ZnO remains positive until solution pH 8.9 (zero-point charge of nano-ZnO), anionic AB 92 dye species develop electrostatic attraction towards the nano-ZnO surface, implying chemisorption (Habib et al., 2012a). As seen from Table 2, the negative values of ΔG of the adsorption process increases with increasing temperature. These findings suggested that the AB 92 dye adsorption onto nano-ZnO was spontaneous.

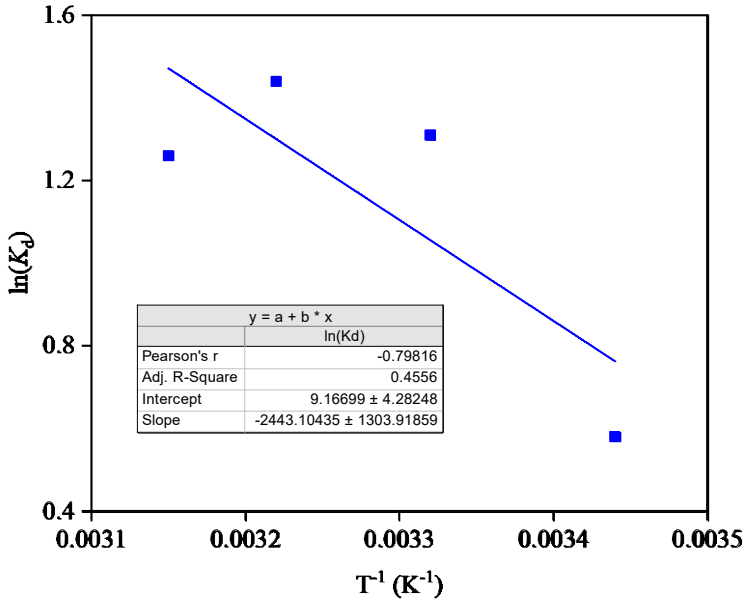

Figure 8. Plot of logK_d versus 1/T for the calculation of ΔH and ΔS for the adsorption of AB 92 dye onto nano-ZnO fiber surface. [AB 92]: 45.32 mgL^{-1}; Nano-ZnO fiber: 1.00 gL^{-1}; Solution pH: 7.0.

Table 2. The thermodynamic parameters for the adsorption process of AB 92 onto the nano-ZnO fiber. [AB 92]: 45.32 mg L^{-1}; Nano-ZnO fiber: 1.00 g L^{-1}; Solution pH: 7.0.

Temperature (K)	1/T (K^{-1})	ΔG (kJmol^{-1})	ΔH (kJmol^{-1})	ΔS (Jmol^{-1} K^{-1})	R (J mol^{-1} K^{-1})
291	0.00344	-1.89	20.32	76.23	8.316
301	0.00332	-2.66			
311	0.00322	-3.42			
317	0.00315	-3.88			

Adsorption in the gas phase and solution phase are two fundamentally distinct processes in terms of thermodynamics. In the gas phase, adsorbate molecules adsorb on the surface of the adsorbent by forming new chemical bonds, resulting in the evolution of heat energy, indicating

that the process is exothermic. On the contrary, adsorption in the solution phase is a different phenomenon. The adsorbate molecules may be aggregated and/or encapsulated in hydration shells depending on the chemical properties of both the adsorbate and adsorbent molecules. Thus, energy is required to break down the aggregates and/or hydration shells for adsorption. Therefore, the system requires a net energy for effective adsorption that provides an endothermic process. On the basis of the obtained thermodynamic parameters, the adsorption process was concluded to be both endothermic and spontaneous (Hameed et. al. 2016; Wu et. al. 2019; Zhang et. al. 2020; Huo et. al. 2019).

3.6. *Adsorption kinetics*

Figure 9 depicts the plot of q_t vs. time that provides the values of the constants of pseudo first order, pseudo second order and Elovich adsorption kinetics. All the parameters are tabulated in Table 3.The results show that the rate constant (k_1) of the pseudo first-order reaction increases with increasing dye concentration (Table 3). The R^2 values are quite lower from unity as well, meaning the pseudo first order kinetic model did not fit the adsorption data properly.

For pseudo second order adsorption kinetics, Figure 9(b) provides k_2 and q_e for the adsorption of different concentrations of AB 92 onto the nano-ZnO fiber. Herein, the rate constant, k_2, also decreases as a function of dye concentration (Table 3). It is noted that the values of R^2 were quite close to unity but decreasing with increasing concentrations of AB 92. Such events are likely to be observed in both adsorption and chemical kinetics. Because there are a maximum number of adsorption sites available at the beginning, the adsorbate molecules adsorb onto the adsorbent surfaces at a faster rate. As the number of active sites for a fixed amount of adsorbent decreases with time, so does the rate of adsorption. Based on the findings, it is concluded that the adsorption of AB 92 onto the nano-ZnO fiber follows pseudo second order rather than pseudo first order kinetics (Nethaji et al., 2013; Mohamed et al., 2017; Salaimi et al., 2017a; Salaimi et al., 2017b).

According to the Figure 9(c), the R^2 values increased with increasing AB92 concentration for the Elovich kinetic model. The initial adsorption rate, A also increased significantly with increasing AB92 concentration as well (Table 3). This leads the conclusion that, the adsorption process is dependent on the AB92 concentration as the electrostatic chemical interaction between the positively charged nano-ZnO surface and the anionic dye increases with greater concentration of anionic species due to their negative charge. The initial desorption rate, B values were extremely low and became even lower with increasing AB92 concentration indicating stable adsorption process and strong interaction between adsorbent and adsorbate

(Efome. et. al. 2018a; Efome. et. al. 2018b). From the kinetic data, it can be concluded that the adsorption process follows pseudo second order and Elovich kinetic models and with increasing AB92 concentration, the process tends to favor Elovich kinetic model rather than pseudo second order kinetic model providing evidence for the process to be chemisorption.

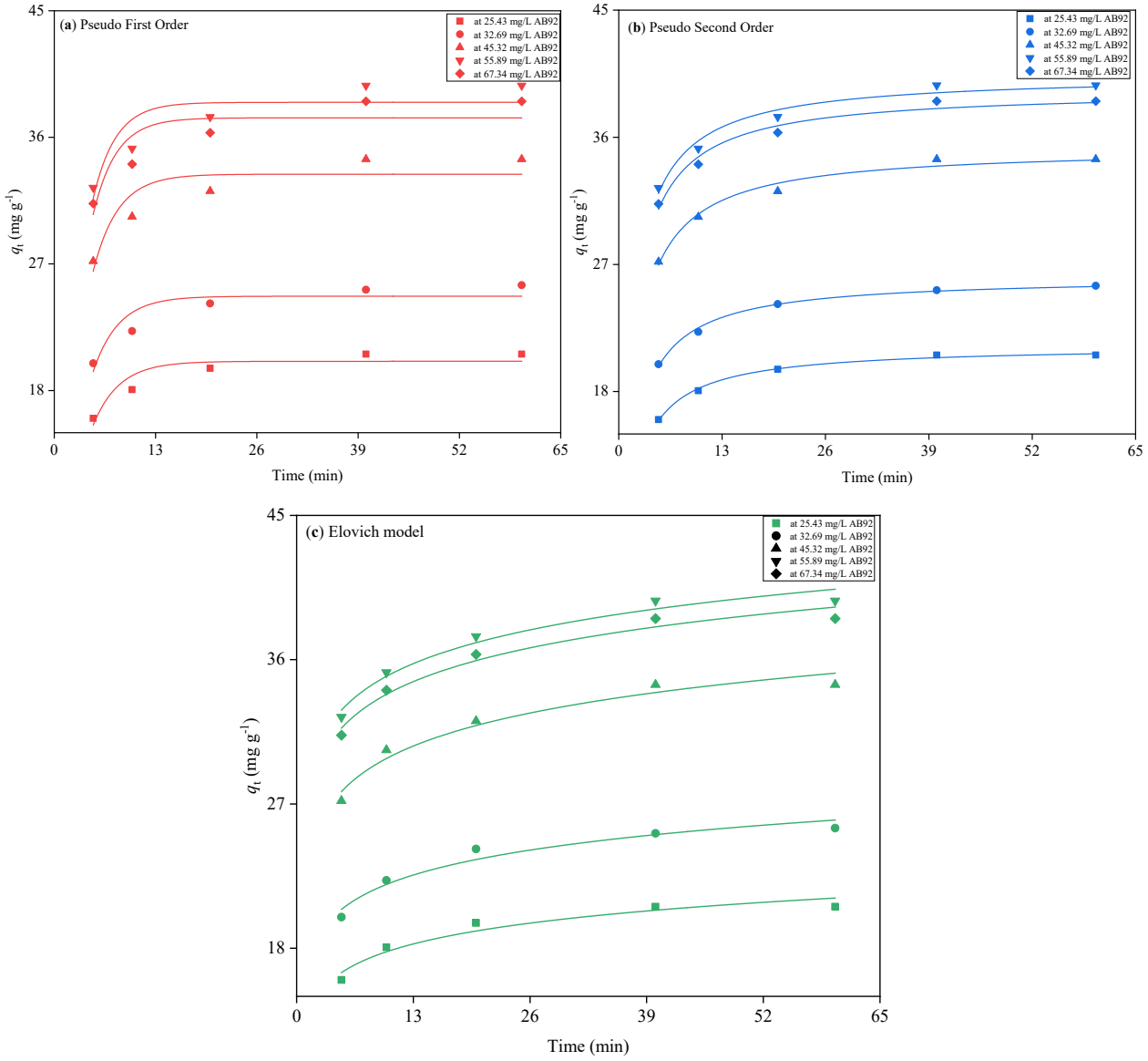

Figure 9. Adsorption kinetics of different concentrations of AB 92 on nano-ZnO fiber of (a) pseudo first-order, (b) pseudo second-order kinetics and (c) Elovich model. Nano-ZnO fiber: 1.00 gL^{-1}; Solution pH: 7.0; Temperature: 298 K.

Table 3. Kinetic parameters of the adsorption of AB 92 dye onto the nano-ZnO fiber. Nano-ZnO fiber: 1.00 g L^{-1}; Solution pH: 7.0; Temperature: 298 K.

Dye conc. (mgL^{-1})	Pseudo first-order kinetics			Pseudo second-order kinetics			Elovich model		
	k_1 (min^{-1})	q_e (mgg^{-1})	R^2	k_2 ($gmg^{-1}min^{-1}$)	q_e (mgg^{-1})	R^2	A ($mgg^{-1}min^{-1}$)	B ($mgg^{-1}min^{-1}$)	R^2
25.43	0.298	20.08	0.8721	0.0282	21.25	0.9950	2500.20	0.534	0.9414
32.69	0.306	24.70	0.8546	0.0239	26.11	0.9948	4057.01	0.446	0.9537
45.32	0.316	33.38	0.8237	0.0184	35.27	0.9827	6845.25	0.337	0.9611
55.89	0.346	38.49	0.7754	0.0183	40.43	0.9748	20886.38	0.329	0.9694
67.34	0.369	41.39	0.7803	0.0182	47.85	0.9755	30583.25	0.329	0.9695

3.7. *Re-usability of nano-ZnO*

The used nano-ZnO was treated with dilute solution of NaOH to investigate its stability as an adsorbent. The treated nano-ZnO was further used for the removal of the AB 92 from the aqueous solution. The prepared nano-ZnO could be effective at least three or four times for the removal of AB92.

As shown in Figure 10, about 76, 75 and 73% of AB92 was removed in the presence of freshly prepared, first re-used and second re-used nano-ZnO (1.00 gL^{-1}) using 45.32 mgL^{-1} dye concentration, respectively at solution pH 7.0 and 298 K. So, it can be concluded that after three or four uses the nano-ZnO can remove at least 70% of AB92 from aqueous solution effectively.

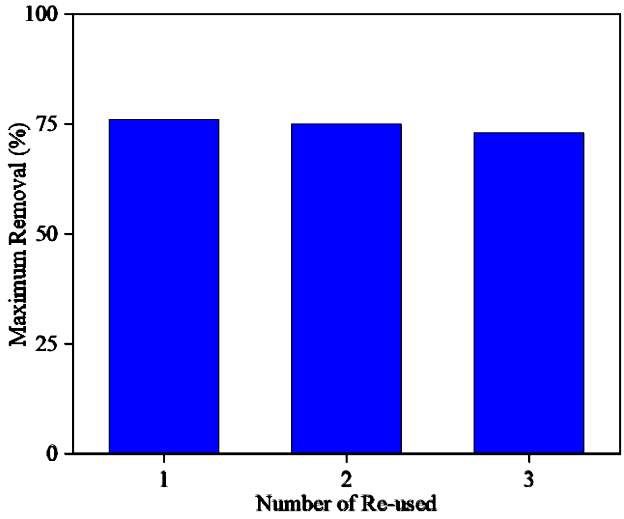

Figure 10. Adsorption of AB92 in the presence of freshly prepared and re-used nano-ZnO fiber (1.00 gL^{-1}) for 45.32 mgL^{-1} of dye concentration at pH 7.0 and 298 K.

3.8. *Mechanism of adsorption and desorption of AB92*

As mentioned above, electrostatic force of attraction plays a vital role for the adsorption of the anionic dye, AB92, onto the positively charged nano-ZnO surface. The surface charge remains positive until the solution pH ≤ 8.9 (Habib et al., 2012a). As the solution pH goes above 8.9, the more available stronger anionic species, OH^-, causes to desorb the adsorbed AB92 molecules from the nano-ZnO surface. A proposed mechanism for this adsorption/desorption process is shown in Scheme 3.

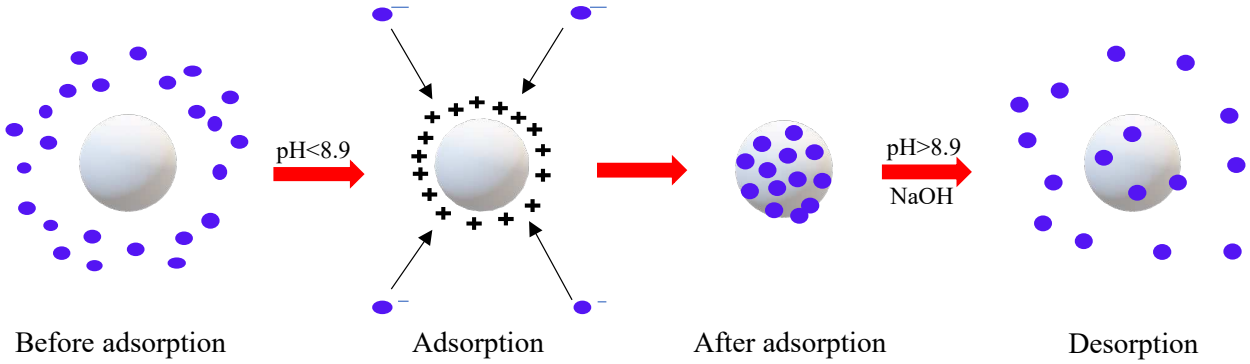

Scheme 3. Proposed mechanism of adsorption and desorption of AB92 in the presence of nano-ZnO fiber.

4. Conclusions

The rapid growth of export-oriented textile industries in Bangladesh discharges untreated effluents into nearby water bodies, causing serious contamination. Many approaches to wastewater depollution, including the desorption method, have already been developed and implemented. Nano-ZnO was produced via precipitation and used as an adsorbent to remove dyes from aqueous solution. SEM, XRD, and FTIR techniques were used to characterize the as-prepared nano-ZnO, which revealed a fiber-like and wurtzite structure. The as-prepared nano-ZnO was applied to the removal of AB 92 dye, a model dye, from aqueous solution to investigate its efficiency. The adsorption study was carried out with variations in dye concentration, solution pH, adsorbent dosage, and temperature in order to optimize the experimental conditions. For 45.32 mgL^{-1} of AB 92, pH 7.0, adsorbent dosage 1.00 gL^{-1} at 311 K, the maximum removal of AB 92 was found to be 78 percent. According to the adsorption studies, the adsorption process of AB 92 onto nano-ZnO strongly followed both the Freundlich

and Temkin's models. The adsorption process appears to be both endothermic and spontaneous, according to thermodynamic studies. The kinetics data revealed that the adsorption process followed pseudo-second order kinetics very closely. The fiber-like nano-ZnO had a high surface area with a positive surface charge (pH≤8.9) and showed enhanced adsorption ability with good recyclability for the removal of the anionic AB92 dye, but only 5% removal for the cationic dyes, MB and RB. It is, therefore, concluded, that the prepared nano-ZnO fiber can be used to remove anionic dyes from aqueous industrial effluents and may be an effective adsorbent in the real world.

Conflict of interest. There are no conflicts of interest declared by the authors.

584 **References**
585
586 Abdelkader, E., Nadjia, L., Rose-Noëlle, V., 2016. Adsorption of Congo red azo dye on
587 nanosized SnO2 derived from sol-gel method. Int. J. Ind. Chem. 7, 53-70.
588 https://doi.org/10.1007/s40090-015-0061-9.
589 Agrawal, S., Tipre, D., Patel, B., and Dave, S., 2014. Optimization of triazo Acid Black 210
590 dye degradation by Providencia sp. SRS82 and elucidation of degradation pathway. Process
591 Biochem. 49, 110–119. doi: 10.1016/j.procbio.2013.10.006.
592 Ahmadi, S., Mohammadi, L., Igwegbe, C.A., Rahdar, S., Banach, A.M., 2018. Application of
593 response surface methodology in the degradation of reactive blue 19 using H_2O_2/MgO
594 nanoparticles advanced oxidation process. Int. J. Ind. Chem. 9(3), 241–253.
595 https://doi.org/10.1007/s40090-018-0153-4.
596 Ahmadi, S., Mohammadi, L., Rahdar, A., Rahdar, S., Dehghani, R., Igwegbe, C. A., Kyzas, G.
597 Z., 2020. Acid Dye Removal from Aqueous Solution by Using Neodymium(III) Oxide
598 Nanoadsorbents. Nanomaterials (Basel, Switzerland), 10(3), 556.
599 https://doi.org/10.3390/nano10030556.
600 Ahmadi, S., Igwegbe, C.A., 2020. Removal of methylene blue on zinc oxide nanoparticles:
601 nonlinear and linear adsorption isotherms and kinetics study. Sigma J. Eng. Nat. Sci. 38(1),
602 289-303. http://eprints.zbmu.ac.ir/id/eprint/3495.
603 Akhtar, M.F., Ashraf, M., Javeed, A., Anjum, A. Ali S.Sharif, A. Akhtar,B. Khan, A. Altaf, I.,
604 2016. Toxicity Appraisal of Untreated Dyeing Industry Wastewater Based on Chemical
605 Characterization and Short Term Bioassays. Bull. Environ. Contam. Toxicol. 96, 502–507.
606 https://doi.org/10.1007/s00128-016-1759-x.
607 Amin, S., Rastogi, R.P., Chaubey, M.G., Jain, K., Divecha, J., Desai, C., Madamwar, D., 2020.
608 Degradation and Toxicity Analysis of a Reactive Textile Diazo Dye-Direct Red 81 by Newly
609 Isolated Bacillus sp. DMS2. Front. Microbiol. 11, 576680.
610 https://doi.org/10.3389/fmicb.2020.576680.
611 Arshadi, M., SalimiVahid, F., Salvacion,J.W.L., Soleymanzadeh, M., 2014. Adsorption studies
612 of methyl orange on an immobilized Mn-nanoparticle: kinetic and thermodynamic. RSC Adv,
613 4, 16005-16017. https://doi.org/10.1039/C3RA47756H.
614 Balarak, D., Zafariyan, M., Igwegbe, C.A., Onyechi, K.K., Ighalo, J.O., 2021. Adsorption of
615 Acid Blue 92 Dye from Aqueous Solutions by Single-Walled Carbon Nanotubes: Isothermal,
616 Kinetic, and Thermodynamic Studies. Environ. Process. 8, 869-888 (2021).
617 https://doi.org/10.1007/s40710-021-00505-3.

M. Belhachemi, F. Addoun, Comparative adsorption isotherms and modeling of methylene blue onto activated carbons, Appl. W. Sci. 1 (2011) 111–117, DOI: 10.1007/s13201-011-0014-1.

Benkhaya S., El Harfi A., 2017. Classifications, properties and applications of textile dyes: a review. Appl. J. Environ. Eng. Sci. 3, 00000-3.https://doi.org/10.48422/IMIST.PRSM/ajees-v3i3.9681.

Benkhaya, S., M'rabet, S., El Harfi, A., 2020. Classifications, properties, recent synthesis and applications of azo dyes. Heliyon. 6(1), e03271. doi:10.1016/j.heliyon.2020.e03271.

Brüschweiler, B.J., Merlot, C., 2017. Azo dyes in clothing textiles can be cleaved into a series of mutagenicaromatic amines which are not regulated yet. Regul.Toxicol.Pharmacol. 88, 214-226. https://doi.org/10.1016/j.yrtph.2017.06.012.

da Silva,P.M., Serna, M.M., Galego,E., Faria Jr. R.N., 2021. The Influence of the Nanostructures on the Dye Adsorptionin Dye Sensitized Solar Cell. Res. Dev. Material Sci. 15, 000859. DOI: 10.31031/RDMS.2021.15.000859.

Degen, A.,Kosec, M., 2000. Effect of pH and impurities on the surface charge of zinc oxide in aqueous solution. J Eur. Ceram. Soc. 20, 667-73.https://doi.org/10.1016/S0955-2219(99)00203-4.

Department of Environment (DoE), Guide for Assessment of Effluent Treatment Plants. Department of Environment, Ministry of Environment and Forest, Bangladesh, 2008, http://old.doe.gov.bd/publication_images/15_etp_assessment_guide.pdf

Dobryszycki, J., Biallozor, S., 2001. On some organic inhibitors of zinc corrosion in alkaline media, Corr. Sci. 43, 1309-1319, DOI: 10.1016/S0010-938X(00)00155-4.

Doulati, A.F., Badii, K.H., Yousef, L.N., Shafaei, S.Z., Mirhabibi, A.R., 2008. Adsorption of Direct Red 80 dye from aqueous solution onto almond shells: efect of pH, initial concentration and shell type. J Hazard Mater 151, 730–737. https://doi.org/10.1016/j.jhazmat.2007.06.048.

Duran, C., Ozdes, D., Gundogdu, A., Senturk, H.B., 2011. Kinetics and isotherm analysis of basic dyes adsorption onto Almond shell (Prunus dulcis) as a low-cost adsorbent. J. Chem. Eng. Data 56, 2136–47. https://doi.org/10.1021/je101204j.

EC, 2009. Commission Regulation (EC) No 552/2009 of 22 June 2009 Amending Regulation (EC) No 1907/2006 of the European Parliament and of the Council on the Registration, Evaluation, Authorisation and Restriction of Chemicals (REACH) as Regards Annex XVII. http://eur-lex.europa.eu/LexUriServ/LexUriServ.do?uri¼OJ:L:2009:164:0007:0031:EN:PDF.

Efome, J.E., Rana, D., Matsuura, T., Lan, C.Q., 2018a. Insight Studies on Metal-Organic Framework Nanofibrous Membrane Adsorption and Activation for Heavy Metal Ions Removal

652 from Aqueous Solution. ACS Appl. Mater. Interfaces 10, 22, 18619–18629.
653 https://doi.org/10.1021/acsami.8b01454.
654 Efome, J.E., Rana, D., Matsuura, T., Lan, C.Q., 2018b. Metal–organic frameworks supported
655 on nanofibers to remove heavy metals. J. Mater. Chem. A, 6, 4550-4555.
656 https://doi.org/10.1039/C7TA10428F.
657 Elmorsi, T.M., Elsayed, M.H., Bakr, M.F., 2017. Enhancing the removal of methylene blue by
658 modified ZnO nanoparticles: kinetics and equilibrium studies. Can. J. Chem. 95, 590-600.
659 dx.doi.org/10.1139/cjc-2016-0456.
660 Elmoubarki, R., Mahjoubi, F.Z., Elhalil, A., Tounsadi, H., Abdennouri, M., Sadiq M., Qourzal,
661 S., Zouhri, A., Barka, N., 2017. Ni/Fe and Mg/Fe layered double hydroxides and their calcined
662 derivatives: preparation, characterization and application on textile dyes removal. J. Mater.
663 Res. Technol. 6, 271-283. https://doi.org/10.1016/j.jmrt.2016.09.007.
664 Ertugay, N., Acar, F.N., 2017. Removal of COD and color from Direct Blue 71 azo dye
665 wastewater by Fenton's oxidation: Kinetic study. Arab. J. Chem. 10, S1158-S1163.
666 http://dx.doi.org/10.1016/j.arabjc.2013.02.009.
667 Freeman, H.S., 2013. Aromatic amines: use in azo dye chemistry. Front. Biosci. Landmark 18,
668 145-164. doi: 10.2741/4093.
669 Freundlich, H., 1906. Adsorption in solutions. J. Phys. Chem. 57, 384-410.
670 Gao, H., Zhao, S., Cheng, X., Wang, X., Zheng, L., 2013. Removal of anionic azo dyes from
671 aqueous solution using magnetic polymer multi-wall carbon nanotube nanocomposite as
672 adsorbent. Chem. Eng. J. 223, 84-90. https://doi.org/10.1016/j.cej.2013.03.004.
673 Govindwar, S. P., Kurade, M. B., Tamboli, D. P., Kabra, A. N., Kim, P. J., and Waghmode, T.
674 R., 2014. Decolorization and degradation of xenobiotic azo dye reactive yellow-84A and textile
675 effluent by Galactomycesgeotrichum. Chemosphere 109, 234–238. doi:
676 10.1016/j.chemosphere.2014.02.009.
677 Habib, A., Hasan, Z., Rahman, S., Alam, A.M.S., 2006. Tuberose Sticks as an Adsorbent in
678 the Removal of Methylene Blue from Aqueous Solution. Pak.J. Anal. Environ. Chem.7, 112-
679 115.
680 https://inis.iaea.org/search/searchsinglerecord.aspx?recordsFor=SingleRecord&RN=3900356
681 7.
682 Habib, A., Islam, R., Chakraborty, M., Serniabad, S., Khan, M.S., Qais, D.S., Quayum, M.E.,
683 Alam, M.A., Ismail, I.M.I., Tabata, M., 2020. Kinetics and mechanism of incorporation of
684 zinc(II) into tetrakis(1-methylpyridium-4-yl)porphyrin in aqueous solution, Arab. J. Chem. 13,
685 6552-6558, DOI: 10.1016/j.arabjc.2020.06.011.

686 Habib, A., Ismail, I.M.I., Mahmood, A.J., Rafiqueullah, M., 2012a. Photocatalytic
687 decolorization of brilliant golden yellow over TiO2 and ZnO suspensions. J. Saudi Chem. Soc.
688 16, 423-429. https://doi.org/10.1016/j.jscs.2011.02.013.
689 Habib, A., Ismail, I.M.I., Mahmood, A.J., Rafiqueullah, M., 2012b. Decolorization and
690 mineralization of Brilliant Golden Yellow (BGY) by Fenton and photo-Fenton processes.
691 African J. Pure Appl. Chem. 6, 153-158.https://doi.org/10.5897/AJPAC10.024.
692 Hameed, A. Dewayanto N. Dongyun, D. Nordin, M. Rahim, M., 2016. Kinetic and
693 thermodynamic of methylene blue adsorption onto zero valent iron supported on mesoporous
694 Silica. Bullet. Chem. Reac. Engin. Cat. 11, 250-261.
695 http://dx.doi.org/10.9767/bcrec.11.2.443.250-261.
696 Han, R., Ding, D., Xu, Y., Zou, W., Wang, Y., Li, Y., Zou, L., 2008. Use of rice husk for the
697 adsorption of congo red from aqueous solution in column mode. Bioresour. Technol. 99, 2938-
698 2946. https://doi.org/10.1016/j.biortech.2007.06.027.
699 Hoda, N., Bayram, E., Ayranci, E., 2006. Kinetic and equilibrium studies on the removal of
700 acid dyes fromaqueous solutions by adsorption onto activated carbon cloth. J. Hazard. Mater.
701 137, 344–351. https://doi.org/10.1016/j.jhazmat.2006.02.009.
702 Hossain, A., Rayhan, A.B.M.S., Raihan, M.J., Nargis, A., Ismail, I.M.I., Habib, A., Mahmood,
703 A.J., 2016. Kinetics of degradation of Eosin Y by one of the advanced oxidation processes
704 (AOPs)-Fenton's process. Am. J. Anal. Chem.7, 863-879. DOI: 10.4236/ajac.2016.712074.
705 Huo, X. Zhang, Y. Zhang, J. Zhou, P. Xie, R. Wei, C. Liu, Y. Wang, N., 2019. Selective
706 adsorption of anionic dyes from aqueous solution by nickel (II) oxide. J. Wa. Sup. Res. Tech.
707 Aqua 68, 171-186. https://doi.org/10.2166/aqua.2019.115.
708 Igwegbe, C.A., Onukwuli, O.D., Ighalo, J.O., Okoye, P.U., 2020. Adsorption of cationic dyes
709 on dacryodesedulis seeds activated carbon modifed using phosphoric acid and sodium chloride.
710 Environ Process 7(4):1151–1171. https://doi.org/10.1007/s40710-020-00467-y.
711 Jethave, G. Fegade, U. Rathod, R. Pawar, J., 2018. Dye pollutants removal from waste water
712 using metal oxide nanoparticle embedded Activated Carbon: An Immobilization study. J. Dis.
713 Sci. Tech. Chem. 40, 563-573.https://doi.org/10.1080/01932691.2018.1472016.
714 Lacasse, K., Baumann, W., 2004. Textile chemicals: environmental data and facts.ISBN 3-
715 540-40815-0. Springer Berlin.
716 Langmuir, I., 1918. Adsorption of gases on plane surfaces of glass,mica and platinum. J. Am.
717 Chem. Soc. 40, 1361-403.https://doi.org/10.1021/ja02242a004.

718 Lei, C., Pi, M., Jiang, C., Cheng, B., Yu, J., 2017. Synthesis of hierarchical porous zinc oxide
719 (ZnO) microspheres with highly efficient adsorption of Congo red. J. Colloid Interface Sci.
720 490, 242-251. https://doi.org/10.1016/j.jcis.2016.11.049.
721 Leila, D., Mar, L.G., Fatima, B., Abddelyamine, N., Ali, B., Nacereddine, H., 2018. Effect of
722 polyethylene glycol and propyltrimethoxysilane on structural and optical properties of zinc
723 oxide nanoparticles synthesized by sol–gel process, J. Theo. Appl. Phy. 12, 159-167, DOI:
724 10.1007/s40094-018-0303-2.
725 Li, Y., Xiao, H., Chen, M., Song, Z., Zhao, Y., 2014. Absorbents based on maleic anhydride-
726 modified cellulose fibers/diatomite for dye removal. J. Mater. Sci. 49, 6696–704.
727 https://doi.org/10.1007/s10853-014-8270-8.
728 Li, Z., Xiong, Y., Xie, Y., 2003. Selected-Control Synthesis of ZnO Nanowires and Nanorods
729 via a PEG-Assisted Route, Inorg. Chem. 42, 8105–8109, DOI: 10.1021/ic034029q.
730 López-Luna, J., Ramírez-Montes, J.E., Martinez-Vargas, S., Martínez, A.I., Mijangos-
731 Ricardez, O.F., González-Chávez, M.C.A., Carrillo-González, R., Solís-Domínguez, F.A.,
732 Cuevas-Díaz, C., Vázquez-Hipólito, V., 2019. Linear and nonlinear kinetic and isotherm
733 adsorption models for arsenic removal by manganese ferrite nanoparticles, SN Appl. Sci. 1,
734 950, DOI: 10.1007/s42452-019-0977-3.
735 Malakootian, M., Mansoorian, H. J., Hosseini, A., Khanjani, N., 2015. Evaluating the efficacy
736 of alumina/carbon nanotube hybrid adsorbents in removing Azo Reactive Red 198 and Blue
737 19 dyes from aqueous solutions. Process Saf. Environ. Prot. 96, 125-137.
738 https://doi.org/10.1016/j.psep.2015.05.002.
739 Mo, C., 2020. Azo Dye Regulations in the United States: An Overview.
740 https://www.compliancegate.com/azo-dye-regulations-united-states/#comments.
741 Mohamed, G., Elshafey, O.I., Fathy, N., 2017. Preparation of Carbonaceous Hydrochar
742 Adsorbents from Cellulose and Lignin Derived from Rice Straw. Egyp. J. Chem. 60, 793-804.
743 DOI: 10.21608/ejchem.2017.1311.1080.
744 Moussavi, G.R., Mahmoudi, M., 2009. Removal of azo and anthraquinone reactive dyes from
745 industrial wastewaters using MgO nanoparticles. J. Hazard. Mater. 168, 806-812.
746 https://doi.org/10.1016/j.jhazmat.2009.02.097.
747 Muslim, M., Habib, A., Islam, T.S.A., Ismail, I.M.I., Mahmood, A.J., 2013. Decolorization of
748 Diazo Dye Ponceau S by Fenton Process. Pak. J. Anal. Environ. Chem. 14, 44-50.
749 http://www.pjaec.pk/index.php/pjaec/article/view/219.

Muslim, M., Habib, A., Mahmood, A.J., Islam, T.S.A., Ismail, I.M.I., 2012. Zinc oxide-mediated photocatalytic decolorization of Ponceau S in aqueous suspension by visible light, Int. Nano Lett. 2, 30. DOI: 10.1186/2228-5326-2-30.

Nargis, A., Habib, A. Rashid, H.-O-., Harun, H.B., Sarker, M.S.I., Jin, R., Liu, G., Liu, W., Al-Razee, A.N.M., Chen, K., Cai, M., 2021. Status of multielement in water of the river Buriganga, Bangladesh: Aquatic chemistry of metal ions in polluted river water,Emerg. Contam. 7, 99-115, https://doi.org/10.1016/j.emcon.2021.03.001.

Nethaji, S., Sivasamy, A., Mandal, A.B., 2013. Adsorption isotherms, kinetics and mechanism for the adsorption of cationic and anionic dyes onto carbonaceous particles prepared from Juglans regia shell biomass. Int. J. Environ. Sci. Technol. 10, 231–242. https://doi.org/10.1007/s13762-012-0112-0.

Ngakou, C.S., Anagho, G.S., Ngomo, H.M., 2019. Non-linear Regression Analysis for the Adsorption Kinetics and Equilibrium Isotherm of Phenacetin onto Activated Carbons, Cur. J. App. Sci. Tech. 36, 1-18, DOI: 10.9734/cjast/2019/v36i430246.

Obiora-Okafo, I.A., Onukwuli, O.D., 2018. Characterization and optimization of spectrophotometric colour removal from dye containing wastewater by coagulation-focculation. Pol. J. Chem. Technol. 20, 49-59. https://doi.org/10.2478/pjct-2018-0054.

Ortega, P.F.R., Trigueiro, J.P.C., Santos, M.R., Denadai Â.M.L., Oliveira, L.C.A., Teixeira, A.P.C., Silva, G.G., Lavall, R.L., 2017. Thermodynamic study of methylene blue adsorption on carbon nanotubes using isothermal titration calorimetry: a simple and rigorous approach. J. Chem. Eng. Data 62, 729-737. https://doi.org/10.1021/acs.jced.6b00804.

Parra, M.R., Haque, F.Z., 2015. Poly (Ethylene Glycol) (PEG)-assisted shape-controlled synthesis of one-dimensional ZnO nanorods, Optik. 126, 1562-1566, DOI: 10.1016/j.ijleo.2015.05.011.

Patra, A.S., Ghorai, S., Ghosh, S., Mandal, B., Pal, S., 2016. Selective removal of toxic anionic dyes using a novel nanocomposite derived from cationically modified guar gum and silica nanoparticles. J. Hazard. Mater. 301, 127-136. https://doi.org/10.1016/j.jhazmat.2015.08.042.

Pavani, K., Kumar, A., 2015. ZnO Nanostructures: Simple Routes of Synthesis. Inter. J. Eng. Res. Technol. 4, 505-508. http://dx.doi.org/10.17577/IJERTV4IS090518

Platzek, T., Lang, C., Grohmann, G., Gi, U.-S., Baltes, W., 1999. Formation of a carcinogenic aromatic amine from an azo dye by human skin bacteria in vitro. Hum. Exp. Toxicol 18, 552-559. https://doi.org/10.1191/096032799678845061.

Rawat, D., Mishra, V., Sharma, R.S., 2016. Detoxification of azo dyes in the context of environmental processes. Chemosphere 155, 591-605. https://doi.org/10.1016/j.chemosphere.2016.04.068.

Redlich, O., Peterson, D.L., 1959. A Useful Adsorption Isotherm, J. Phys. Chem. 63, 1024, DOI: 10.1021/j150576a611.

Salaimi, F., Tahmasobi, K., Karami, C., Jahangiri, A., 2017a. Preparation of Modified nano-SiO_2 by Bismuth and Iron as a novel Remover of Methylene Blue from Water Solution. J. Mex. Chem. Soc. 61, 250-259. DOI: 10.29356/jmcs.v61i3.351.

Salaimi, F., Eskandari, M., Karami, C., 2017b. Investigation of methylene blue adsorption in wastewater using nano-zeolite modified with copper. Desalin. Water Treat. 85, 206-214. Doi: 10.5004/dwt.2017.21248.

Salem, A.N.M., Ahmed, M.A., El-Shahat, M.F., 2016. Selective adsorption of amaranth dye on Fe_3O_4/MgO nanoparticles. J. Mol. Liq. 219, 780-788. https://doi.org/10.1016/j.molliq.2016.03.084.

Saravanan, R., Karthikeyan, S., Gupta, V.K., Sekaran, G., Narayanan, V., Stephen, A., 2013. Enhanced photocatalytic activity of ZnO/CuO nano-composite for the degradation of textile dye on visible light illumination. Mater. Sci. Eng. C 33, 91–98. https://doi.org/10.1016/j.msec.2012.08.011.

Saravanan, R., Gupta, V.K., Narayanan, V., Stephen, A., 2014. Visible light degradation of textile efuent using novel catalyst ZnO/γ-Mn_2O_3. J. Taiwan Inst. Chem. Eng. 45, 1910–1917. https://doi.org/10.1016/j.jtice.2013.12.021.

Somasundaran, P., Runkana, V., 2005. Investigation of the flocculation of colloidal suspensions by controlling adsorbed layer microstructure and population balance modeling. Chem. Eng. Res. Des. 83, 905-914. https://doi.org/10.1205/cherd.04345.

Sun, J., Song, T., Wang, J., Guo, X., Su, L., Tu, W., 2020. Enhanced selective adsorption ability of Cu_2O nanoparticles for anionic dye by sulfur incorporation. SN Appl. Sci. 2, 1103. https://doi.org/10.1007/s42452-020-2914-x.

Tan, L., Ning, S., Zhang, X., and Shi, S., 2013. Aerobic decolorization and degradation of azo dyes by growing cells of a newly isolated yeast Candida tropicalis TL-F1. Bioresour. Technol. 138, 307-313. doi: 10.1016/j.biortech.2013.03.183.

Tan, L., He, M., Song, L., Fu, X., and Shi, S., 2016. Aerobic decolorization, degradation and detoxification of azo dyes by a newly isolated salt-tolerant yeast Scheffersomycesspartinae TLHS-SF1. Bioresour. Technol. 203, 287-294. doi: 10.1016/j.biortech.2015.12.058.

Tang, L. Cai, Y. Yang, G. Liu, Y. Zeng, G. Zhou, Y. Li, S. Wang, J. Zhang, S. Fang, Y. He, Y., 2014. Cobalt nanoparticle-embedded magnetic ordered mesoporous carbon for highly effective adsorption of rhodamine B. App. Surf. Sci. Els. Chem. 314, 746-753.https://doi.org/10.1016/j.apsusc.2014.07.060.

Temkin, M.J., Pyzhev, V.,1940. Recent modifications to Langmuirisotherms. Acta Physiochim. USSR 12, 217-22. https://www.sid.ir/En/Journal/ViewPaper.aspx?ID=312965.

Tshabalala, M.A., Dejene, B.F., Swart, H.C., 2012. Synthesis and characterization of ZnO nanoparticles using polyethylene glycol (PEG), Physica B Cond. Matter 407, 1668-1671, DOI: 10.1016/j.physb.2011.09.113.

Wikipedia, https://en.wikipedia.org/wiki/Proton_affinity.

Wang, Z., Yin, P., Qu, R., Chen, H., Wang, C., Ren, S., 2013. Adsorption kinetics, thermodynamics and isotherm of Hg(II) from aqueous solutions using buckwheat hulls from Jiaodong of China, Food Chem. 136, 1508-1514, DOI: 10.1016/j.foodchem.2012.09.090.

Wu, J. Xia, A. Chen, C. Feng, L. Su, X. Wang, X., 2019. Adsorption thermodynamics and dynamics of three typical dyes onto bio-adsorbent spent substrate of Pleurotuseryngii. Int J Environ Res Public Health. 16, 679. doi: 10.3390/ijerph16050679.

Xiong, H.-M., Shchukin, D.G., Möhwald. H., Xu, Y., Xia, Y.-Y., 2009. Sonochemical synthesis of highly luminescent zinc oxide nanoparticles doped with magnesium(II). Angew Chem. Int. Edit. 48, 2727-2731.DOI: 10.1002/anie.200805590.

Yakar, A., Ünlü, A., Yeşilçayır, T., Bıyık, I., 2020. Kinetics and thermodynamics of textile dye removal by adsorption onto iron oxide nanoparticles. Nanotechnol. Environ. Eng. 5, 6. https://doi.org/10.1007/s41204-020-0068-0.

Zafar, M.N., Dar, Q., Nawaz, F., Zafar, M.N., Iqbal, M., Nazar, M.F., 2019. Effective adsorptive removal of azo dyes overspherical ZnO nanoparticles. J. Mater. Res. Technol. 8, 713-725. https://doi.org/10.1016/j.jmrt.2018.06.002.

Zhang, Y., Wang, D., Zhang, X., Qu, F., 2013. Template-free synthesis of porous Cu_2O nanospheres at room temperature and investigation on their adsorption property. J Nanomater 2013:1–5. https://doi.org/10.1155/2013/378919.

Zhang, H. Wu, D. Huang, Q. Liu, Z. Luo, X. Xiong, S. Yin, T., 2020. Adsorption kinetics and thermodynamics of yeast β-glucan for off-odor compounds in silver carp mince. Food Chem. 319, 126232. DOI: 10.1016/j.foodchem.2020.126232.